INL/JOU-21-64836-Revision-0

A two-phase three-field modeling framework for heat pipe application in nuclear reactors

January 2022

Shanbin Shi, Yang Liu, Ilyas Yilgor, Piyush Sabharwall

Changing the World's Energy Future

INL is a U.S. Department of Energy National Laboratory operated by Battelle Energy Alliance, LLC

INL/JOU-21-64836-Revision-0

A two-phase three-field modeling framework for heat pipe application in nuclear reactors

Shanbin Shi, Yang Liu, Ilyas Yilgor, Piyush Sabharwall

January 2022

Idaho National Laboratory
Idaho Falls, Idaho 83415

http://www.inl.gov

Prepared for the
U.S. Department of Energy
Under DOE Idaho Operations Office
Contract DE-AC07-05ID14517

A Two-Phase Three-Field Modeling Framework for Heat Pipe Application in Nuclear Reactors

Shanbin Shi[1], Yang Liu[2], Ilyas Yilgor[1], Piyush Sabharwall[3]

[1]Department of Mechanical, Aerospace, and Nuclear Engineering,
Rensselaer Polytechnic Institute
110 8th Street, Troy, NY 12180, United States

[2]Nuclear Engineering Program, Department of Mechanical Engineering
Virginia Tech
635 Price Fork Road, Blacksburg, VA 24061, United States

[3]Idaho National Laboratory
2525 Fremont Ave, Idaho Falls, ID 83402, United States

ABSTRACT

Heat pipes and two-phase thermosyphons are highly efficient heat transfer devices utilizing continuous evaporation and condensation of working fluid for two-phase heat transport in closed systems. Because of the nearly isothermal and fully passive phase-change heat transfer mechanism, heat pipes and thermosyphons have found many applications in nuclear engineering, space technologies, and other energy systems. High-temperature heat pipes are used in nuclear microreactors to remove fission power from the primary system and are coupled with power conversion systems or process heat applications. Modeling of the two-phase flow phenomena inside a heat pipe is essential to its design and safety analysis. In this study, a comprehensive one-dimensional two-phase three-field flow model has been developed for the analysis of heat pipes in normal operation conditions and transients. The conservation or field equations of mass, momentum, and energy were developed for the liquid film, vapor, and droplet. In addition, constitutive models or correlations were reviewed thoroughly and provided for the closure of the three-field equations. Specific constitutive equations regarding interfacial mass and heat transfer at two interfaces, namely film-gas interface and gas-droplet interface, were reviewed for droplet entrainment and deposition rates as well as film and droplet evaporation rates. Additionally, mechanistic correlations of annular flow film thickness were recommended for the modeling of the thermosyphons without a wick as a critical constitutive correlation. Furthermore, experimental data needs from new experiments using a prototype working fluid or surrogate fluids for the model validation of high-temperature heat pipes in microreactors were recommended for future research.

KEYWORDS

Heat pipes, Thermosyphons, Two-phase Three-field flow, One-dimensional Model, Dimensionless Numbers

1. INTRODUCTION

A heat pipe or a thermosyphon operates passively upon the natural circulation developed inside the pipe [1-4]. The difference between a heat pipe and a thermosyphon is that the former includes wicks and the latter is wickless. Figure 1 shows a typical heat pipe schematic with a wicking structure. As can be seen, the heat pipe mainly consists of three sections: the evaporator, adiabatic section, and condenser. With a closed cycle of phase change heat transfer, heat can be transferred from the evaporator (heat source) to the condenser (heat sink). Inside the heat pipe, vapor generated due to boiling or evaporation flows to the adiabatic section and further into the condenser, where it is condensed to form the liquid film flowing back to the evaporator. During stable operating conditions, annular countercurrent two-phase flow regime dominates the flow inside the heat pipe. However, it is important to note that the operations of heat pipes and thermosyphons are not exactly the same. The heat pipe promotes the liquid flow from the condenser to the evaporator with both capillary and gravitational forces due to the existence of wicks, whereas the thermosyphon mainly relies on the gravitational force.

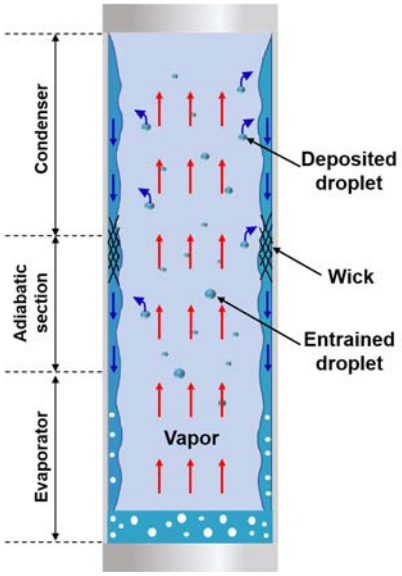

Figure 1. Schematic of a Two-phase Closed Heat Pipe.

The accurate modeling of two-phase flow and phase change heat transfer is of paramount importance to various thermal systems utilizing heat pipes such as heat pipe cooled microreactors [5-7] and space reactor systems [8,9]. The theoretical and numerical simulations of heat pipes can be divided into three categories [10]. The first category consists of various operating limits of flow dynamics and heat transfer as well as developed dimensionless numbers [11-13]. Key operating limits such as viscous limit, sonic limit, entrainment limit, wicking limit, and boiling limit have been derived and summarized by several researchers [1-4]. These developed limitation correlations or dimensionless numbers are very useful for designing heat pipes and heat pipe test facilities. The appropriate operational temperature range can be determined for a given heat pipe design with a selected working fluid.

The second category of modeling approach uses conservation equations for analyzing and formulating two-phase flows under both steady-state and transient conditions inside heat pipes, which is categorized as a full flow model by Mueller and Tsvetkov [10]. To simulate various transients, Reed and Tien formulated one-dimensional governing equations and correlations for the steady-state and transient operation of a two-phase closed thermosyphon [14]. Wall shear stress, interfacial friction, and heat transfer coefficient correlations were used as constitutive equations. The calculation of the liquid film thickness was based on the classical Nusselt solution for laminar condensation on a plate [14,15]. Their numerical predictions of condensate film thickness and flooding predictions agreed well with steady-state experimental data. Harley and Faghri presented a transient two-dimensional thermosyphon model for the vapor flow coupled with unsteady heat conduction in the wall, and the falling film was modeled using a quasi-steady Nusselt-type solution [16]. The falling condensate film in the entire thermosyphon was simulated by taking into account variable vapor condensation rate, interfacial friction, and vapor pressure drop. The model was validated with low-temperature experimental data. In addition, the effects of vapor compressibility were investigated for a high-temperature vertical stainless-steel/sodium thermosyphon operation. Tournier and El-Genk developed a two-dimensional heat pipe transient analysis model (HPTAM) for simulating operation of heat pipes [17]. HPTAM code predictions include heat pipe transients and axial distribution of the liquid and vapor pressures, capillary pressure at the liquid and vapor interfaces, etc. Later, HPTAM's capability was further expanded by including freeze-and-thaw model and the modeling of free-molecular and transition flow regimes for simulating startup of low-temperature heat pipes and high-temperature heat pipes from a frozen state, respectively [18].

Finally, the third category utilizes a simplified network system of conductors, namely thermal resistance model, for representing the heat transfer processes inside a heat pipe [3,13,19] without solving governing equations for both fluid fields. The thermal resistance model was implemented successfully for steady-state

heat pipe analysis [3]. Most recently, this method was used in the System Analysis Module (SAM) for the analysis of heat pipe cooled microreactors [20], such as temperature distributions and heat transport capacity of heat pipes.

Since heat pipe technologies have recently been adopted in the design of nuclear microreactors, no general agreement has been reached in nuclear engineering on the modeling approaches and corresponding complexities, i.e., one-dimensional or three-dimensional formulations that could be used in nuclear reactor design and safety analysis. Among the three categories of the heat pipe modeling approaches mentioned above, the second category based on governing equations has greater flexibility and potential for future licensing of the advanced nuclear reactors utilizing heat pipes for heat removal, while the other two categories could have significant difficulties in simulating complex flow dynamics and phase change inside the heat pipes, especially in transients. To account for various physics involved, constitutive models and correlations are essential to be solved with the governing equations for fluids. Therefore, the accuracy of the implemented constitutive models or correlations is very important to the modeling of thermo-fluid dynamics in two-phase flows. With the advancement of two-phase flow research in the past two decades, more high-quality experimental data have been obtained for a far better understanding of the complex two-phase flows of high void fractions such as the annual flows, which actually dominate the flow dynamics in heat pipes. In addition, there has been research work performed to investigate evaporation regimes and dynamic characteristics in heat pipes or thermosyphons, such as evaporation regimes in narrow space [21], gravity-capillary evaporation regimes [22], and dynamic performance analysis on start-up transients [23]. Unfortunately, appropriate heat pipe two-phase flow modeling approaches and applicable constitutive models have not been systematically presented and discussed in nuclear engineering.

Therefore, the present paper adopts the modeling strategy based on the governing equations combined with the state-of-the-art two-phase flow modeling approaches. As illustrated in Fig. 1, the liquid droplets and liquid film can co-exist inside heat pipes or thermosyphons due to entrainment and deposition. The droplet field might be of critical importance to the heat pipe operations in the microreactors, which normally feature small outer pipe diameter such as 1.775 cm with a high aspect ratio in one design [7]. Thus, a wavy liquid film can be entrained into the upward vapor flow due to relatively high gas velocity. However, in previous heat pipe two-phase flow modeling, the liquid field governing equations did not differentiate two forms of the liquid phase, namely the liquid droplets and liquid film. Therefore, existing models considering only liquid film and vapor fields could have difficulties in simulating droplet entrainment and deposition inside the heat pipes and thermosyphons.

In this paper, a comprehensive one-dimensional two-phase three-field model has been developed for a relatively simplified modeling of heat pipes because of their high aspect ratios in nuclear reactor applications. In addition, appropriate constitutive models or correlations are recommended for the closure of the governing equations. The developed three-field model offers greater flexibility in modeling complexity and therefore is applicable in a wide range of conditions. This modeling paper is outlined as follows: Section 2 presents the mathematical formulation of the governing equations (field equations) and constitutive equations for the heat pipes and thermosyphons. A detailed review of the state-of-the-art constitutive equations is carried out to complete the equation system. The modeling requirement of high-temperature heat pipes using liquid metals as working fluids is discussed. In addition, dimensionless parameters are introduced for scaling analysis of heat pipes. Key conclusions of this research are summarized in Section 3.

2. ONE-DIMENSIONAL THREE FIELD MODEL

2.1. Conservation Equations

Ishii rigorously derived the classical two-fluid model using a time-averaging method [24,25]. In Ishii's model, all gas fields including various bubbles and annular gas core are considered in one set of conservation equations, whereas the liquid fields including continuous liquid and dispersed droplets are considered in another equation set. To account for various two-phase flow regimes including the annular flow, the four-field two-fluid model has been proposed in the literature [26,27]. Four sets of conservation equations could be given to four fluid fields including the continuous liquid, dispersed liquid, continuous gas and dispersed gas. Liu et al. [28] further extended Ishii's work and developed the theoretical foundation of a generic multi-field model. In this model, any fluid field of similar characteristics can be described by a set of conservation equations. Both the interfacial transfer terms and inter-field transfer terms appear in the multi-field model. Based on this work, a three-field model can be developed by considering the specific geometry and operating conditions in heat pipes or thermosyphons. The three fields that are important to this problem include the gas core, liquid film, and droplet.

Figure 2 shows a diagram for a simplified heat pipe model with a wick. Within the heat pipe, the vapor flows upward to the condenser (vapor core), while the condensate flows downward inside the wick along the heat pipe wall with a vertical configuration. The droplets in the gas core might deposit into the liquid film. Conversely, they might be entrained into the gas core from the wavy liquid film. The one-dimensional modeling of the two-phase flows in a heat pipe in this study is based on the following assumptions:

(1) Wick is filled with liquid, no bubbles or vapor.

(2) Liquid film does not extend outside the wick layer.

(3) Liquid only exists in the form of droplets in the gas core, deposition and entrainment could occur.

(4) One-dimensional (1-D) model assuming uniform velocity profile, distribution parameters may not be considered.

(5) Normal stress may be neglected compared with wall shear stress.

(6) All the parameters in the following equations are 1-D area-averaged quantities.

It should be noted that the present modeling framework is developed specifically for the phase change induced countercurrent annular flow which exists in heat pipes and thermosyphons.

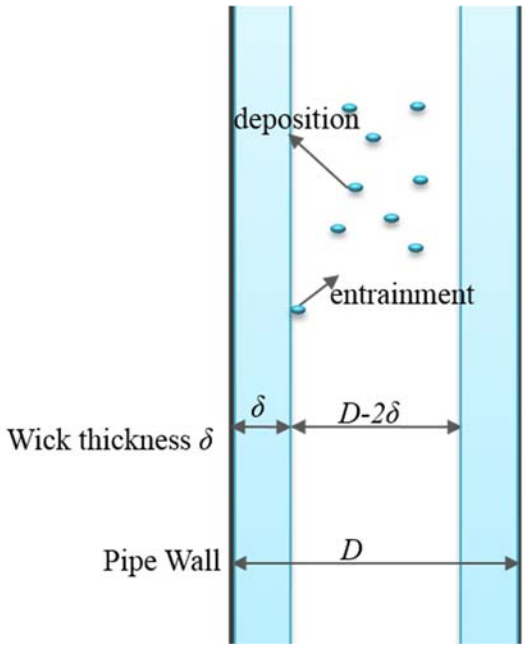

Figure 2. Annular Flow Model in a Heat Pipe.

Continuity equation for the film:

$$\frac{\partial\left(\varepsilon\rho_f\right)}{\partial t}+\frac{\partial\left(\varepsilon\rho_f v_f\right)}{\partial z}=\left(\dot{d}-\dot{\varepsilon}-\dot{\gamma}_f\right)\frac{4\left(D-2\delta\right)}{\left[D^2-\left(D-2\delta\right)^2\right]} \tag{1}$$

where, ε, δ, $\dot{d}$, $\dot{\varepsilon}$, and $\dot{\gamma}_f$ denote the wick porosity, wick thickness, droplet deposition rate per unit film surface area, droplet entrainment rate per unit film surface area, and film evaporation rate per unit film

surface area, respectively. It should be noted that for the modeling of the two-phase thermosyphons without a wick, the wick porosity ε is equal to one and δ becomes a liquid film thickness.

Continuity equation for the vapor:

$$\frac{\partial\left[\left(1-\alpha_d\right)\rho_g\right]}{\partial t}+\frac{\partial\left[\left(1-\alpha_d\right)\rho_g v_g\right]}{\partial z}=\frac{4\dot{\gamma}_f}{\left(D-2\delta\right)}+\dot{\Gamma}_d \tag{2}$$

Continuity equation for the droplet:

$$\frac{\partial\alpha_d\rho_d}{\partial t}+\frac{\partial\left(\alpha_d\rho_d v_d\right)}{\partial z}=\left(-\dot{d}+\dot{\varepsilon}\right)\frac{4}{\left(D-2\delta\right)}-\dot{\Gamma}_d \tag{3}$$

where, $\dot{\Gamma}_d$ and α_d are the droplet evaporation rate per unit vapor-droplet mixture volume and droplet fraction in the gas core region, respectively.

Momentum equation for the film:

$$\begin{aligned}\left[\frac{\partial}{\partial t}\left(\varepsilon\rho_f v_f\right)+\frac{\partial}{\partial z}\left(\varepsilon\rho_f v_f v_f\right)\right]=&\varepsilon\left(-\frac{\partial p_f}{\partial z}-\rho_f g_z\right)+M_{wick}\\&+\tau_{\mathrm{i}}\varepsilon_i\frac{4\left(D-2\delta\right)}{\left[D^2-\left(D-2\delta\right)^2\right]}-\tau_{\mathrm{w}}\varepsilon_w\frac{4D}{\left[D^2-\left(D-2\delta\right)^2\right]}\\&+\left(\dot{d}v_d-\dot{\varepsilon}v_f-\dot{\gamma}_f v_f\right)\frac{4\left(D-2\delta\right)}{\left[D^2-\left(D-2\delta\right)^2\right]}\end{aligned} \tag{4}$$

where, ε_i, ε_w, τ_{i}, τ_{w}, and M_{wick} denote the liquid area fraction at the wick-gas interface, liquid area fraction at the wall, interfacial shear between liquid and gas, wall shear, and drag force term between the liquid and wick, respectively. Additionally, frictional pressure drop for the film in porous media can be written as [4]

$$-\left.\frac{dp}{dz}\right|_{wick}=M_{wick}=\frac{\varepsilon v_f\mu}{K} \tag{5}$$

where, v_f and μ are the liquid velocity and liquid viscosity, respectively. K is the wick permeability and can be calculated from

$$K = \frac{\varepsilon D_h^2}{2f\,\mathrm{Re}} \tag{6}$$

here, D_h and f are the hydraulic diameter and Fanning friction factor, respectively. Permeability depends on the wick structure and Reynolds number. The flow in the heat pipe wick structure is laminar due to low liquid velocity while the permeability *K* only depends on wick geometry [1]. By substituting Eq. (5) into Eq. (4), one obtains

$$\begin{aligned}\left[\frac{\partial}{\partial t}\left(\varepsilon\rho_f v_f\right)+\frac{\partial}{\partial z}\left(\varepsilon\rho_f v_f v_f\right)\right] &= \varepsilon\left(-\frac{\partial p_f}{\partial z}-\rho_f g_z\right)-\frac{\varepsilon v_f \mu}{K} \\ &+\tau_{\mathrm{i}}\varepsilon_i\frac{4\left(D-2\delta\right)}{\left[D^2-\left(D-2\delta\right)^2\right]}-\tau_{\mathrm{w}}\varepsilon_w\frac{4D}{\left[D^2-\left(D-2\delta\right)^2\right]} \\ &+\left(\dot{d}v_d-\dot{\varepsilon}v_f-\dot{\gamma}_f v_f\right)\frac{4\left(D-2\delta\right)}{\left[D^2-\left(D-2\delta\right)^2\right]}\end{aligned} \tag{7}$$

It should be noted that based upon the wick structure and the method by which the permeability is analytically derived or measured, the wick permeability may account for the wall shear stress as well. In which case, the wall shear stress term in Eq. (7) may be dropped.

Momentum equation for the vapor:

$$\begin{aligned}\frac{\partial\left[\left(1-\alpha_d\right)\rho_g v_g\right]}{\partial t}+\frac{\partial}{\partial z}\left[\left(1-\alpha_d\right)\rho_g v_g v_g\right] &= \left[-\left(1-\alpha_d\right)\frac{\partial p_g}{\partial z}-\left(1-\alpha_d\right)\rho_g g_z\right] \\ &-\frac{4\varepsilon_i\tau_{\mathrm{i}}}{\left(D-2\delta\right)}-\frac{4\left(1-\varepsilon_i\right)\tau_{i,wick}}{\left(D-2\delta\right)}-M_{iD}+\frac{4\dot{\gamma}_f}{\left(D-2\delta\right)}v_f+\dot{\Gamma}_d v_d\end{aligned} \tag{8}$$

where, M_{iD} and $\tau_{i,wick}$ are the drag force term between droplets and gas, and shear between gas and wick at the interface, respectively.

Momentum equation for the droplet:

$$\frac{\partial(\alpha_d \rho_d v_d)}{\partial t} + \frac{\partial}{\partial z}(\alpha_d \rho_d v_d v_d) = -\alpha_d \frac{\partial p_d}{\partial z} - \alpha_d \rho_d g_z + M_{iD} - \frac{4}{(D-2\delta)} \dot{d} v_d + \frac{4}{(D-2\delta)} \dot{\varepsilon} v_f - \dot{\Gamma}_d v_d \tag{9}$$

Energy equation for the film:

$$\left[\frac{\partial}{\partial t}(\varepsilon \rho_f h_f) + \frac{\partial}{\partial z}(\varepsilon \rho_f v_f h_f)\right] = k_{eff} \frac{\partial^2 T_f}{\partial z^2} + q''_{wall} \frac{4D}{\left[D^2 - (D-2\delta)^2\right]} + q''_{f,fi} \frac{4(D-2\delta)}{\left[D^2 - (D-2\delta)^2\right]} + \left(\dot{d} h_d - \dot{\varepsilon} h_f - \dot{\gamma}_f h_{f,fi}\right) \frac{4(D-2\delta)}{\left[D^2 - (D-2\delta)^2\right]} \tag{10}$$

where, q''_{wall}, $q''_{f,fi}$, $h_{f,fi}$, and k_{eff} are the wall heat flux, heat flux on the liquid side of the film interface, enthalpy on the liquid side of the film interface, effective thermal conductivity considering the wick effect, respectively.

Energy equation for the vapor:

$$\frac{\partial\left[(1-\alpha_d)\rho_g h_g\right]}{\partial t} + \frac{\partial}{\partial z}\left[(1-\alpha_d)\rho_g v_g h_g\right] = \frac{4\dot{\gamma}_f}{(D-2\delta)} h_{g,fi} + \frac{4}{(D-2\delta)} q''_{g,fi} + \dot{\Gamma}_d h_{g,di} + a_{i,d} q''_{g,di} \tag{11}$$

where, $h_{g,fi}$, $q''_{g,fi}$, $h_{g,di}$, and $q''_{g,di}$ denote the enthalpy on the gas side of the film interface, heat flux on the gas side of the film interface, enthalpy on the gas side of the droplet interface, and heat flux on the gas side of the droplet interface, respectively.

Energy equation for the droplet:

$$\frac{\partial(\alpha_d \rho_d h_d)}{\partial t} + \frac{\partial}{\partial z}(\alpha_d \rho_d v_d h_d) = a_{i,d} q''_{d,di} - \dot{\Gamma}_d h_{d,di} - \dot{d} h_d \frac{4}{(D-2\delta)} + \dot{\varepsilon} h_f \frac{4}{(D-2\delta)} \tag{12}$$

where, $a_{i,d}$, $q''_{d,di}$, and $h_{d,di}$ are the droplet interfacial area concentration, heat flux on the liquid side of the droplet interface, and enthalpy on the liquid side of the droplet interface, respectively.

The above set of conservation equations consider a wick structure inside the heat pipe. If the two-phase flows in a wickless thermosyphon is modeled, the drag force term between the liquid and wick M_{wick} and the shear between gas and wick at the interface $\tau_{i,wick}$ can be dropped from the equations.

Additionally, the following relations representing macroscopic jump conditions between interfacial heat transfer terms should be conserved at two interfaces.

Jump conditions at the film interface:

$$\dot{\gamma}_f h_{g,fi} - \dot{\gamma}_f h_{f,fi} + q''_{g,fi} + q''_{f,fi} = 0 \tag{13}$$

Jump conditions at the droplet interface:

$$a_{i,d} q''_{d,di} - \dot{\Gamma}_d h_{d,di} + \dot{\Gamma}_d h_{g,di} + a_{i,d} q''_{g,di} = 0 \tag{14}$$

In addition, the momentum jump condition in the radial direction at the liquid-vapor interface can be expressed as

$$\left(p_f - p_g\right) + 2\frac{\sigma}{R_c} + \dot{\gamma}_f^2 \left(\frac{1}{\varepsilon \rho_f} - \frac{1}{\rho_g}\right) = 0 \tag{15}$$

where, σ and R_c are the liquid surface tension and the curvature of the liquid meniscus, respectively.

2.2. Constitutive Models and Relations

For the closure of the conservation equations presented above, constitutive models or correlations are required such as the equation of state to specify fluid properties, wall and interfacial shear stresses, and liquid-film heat transfer coefficients. Many of these constitutive models have been presented in various textbooks [1-3,29-31] and existing literature [14,28,32-38]. Therefore, they will not be repeated in this paper. Instead, due to the introduction of the droplet field into the conventional two-fluid model [31], important constitutive equations accounting for interfacial mass and heat transfer are discussed in this section.

2.2.1. Droplet entrainment rate

Countercurrent vertical annular flows are expected in the thermosyphons or heat pipes during normal operating conditions. Due to the lack of a wick structure, an important operating limit of thermosyphons is

the entrainment limit beyond inception of entrainment. An understanding of the conditions leading to entrainment of a downward liquid film flow into the upward vapor flow is of significant importance to the mass and heat transfer modeling and stable operation of the two-phase thermosyphons. In the countercurrent film flow, the entrainment mechanism is closely associated with the flooding phenomenon. When the flooding condition is reached, waves of large amplitude can be separated from the film to form a bulge or even to create a liquid bridge connecting the walls. Summarized by Ishii and Grolmes [39], there are basically five types of entrainment mechanisms as shown in Fig. 3. Among these five different mechanisms, Types 1, 2, 4 and 5 could be considered important in the two-phase thermosyphons.

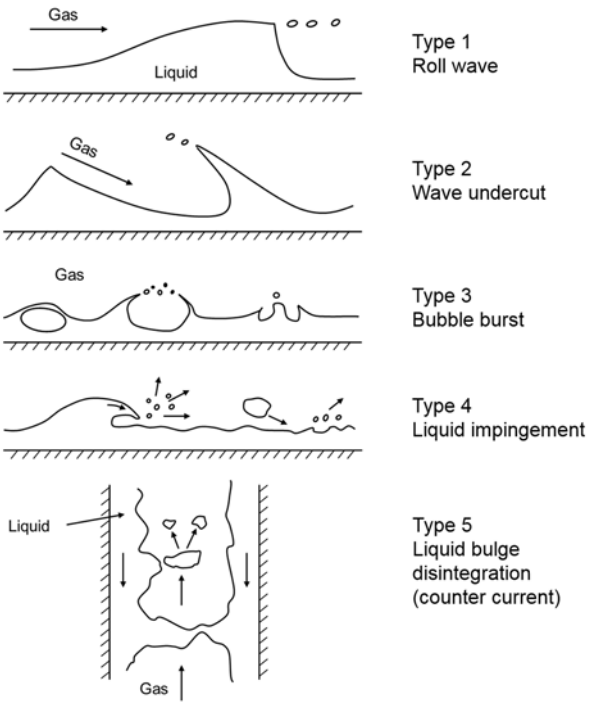

Figure 3. Different Entrainment Mechanisms [39].

First, the inception of the droplet entrainment is determined based on the critical gas velocity. Meanwhile, it is related to the liquid flow direction, liquid Reynolds number Re_f, and the viscosity number N_{μ_f}. Ishii and Grolmes [39] obtained the droplet entrainment inception criteria by considering the shearing off roll-wave crests in the range $2 < \mathrm{Re}_f < 1,635$ for the downward flow, which is given by

$$\begin{cases} \dfrac{\mu_f j_g}{\sigma}\sqrt{\dfrac{\rho_g}{\rho_f}} \geq 11.78 N_{\mu_f}^{0.8}\,\mathrm{Re}_f^{-1/3} & \text{for} \quad N_{\mu_f} \leq \dfrac{1}{15} \\ \dfrac{\mu_f j_g}{\sigma}\sqrt{\dfrac{\rho_g}{\rho_f}} \geq 1.35\,\mathrm{Re}_f^{-1/3} & \text{for} \quad N_{\mu_f} > \dfrac{1}{15} \end{cases} \tag{16}$$

where, the liquid viscosity number N_{μ_f} is given by

$$N_{\mu_f} = \frac{\mu_f}{\left(\rho_f \sigma \sqrt{\dfrac{\sigma}{g\Delta\rho}}\right)^{1/2}} \tag{17}$$

And the liquid film Reynolds number is defined by

$$\mathrm{Re}_f = \frac{4\rho_f v_f \delta}{\mu_f} = \frac{\rho_f j_f D_h}{\mu_f} \tag{18}$$

The droplet entrainment rate has been modeled in a number of studies in the past [40-43]. The classical correlation developed by Kataoka and Ishii [44] is presented below as it can be used to predict both developing and well-developed annular flows.

For the developing region $(\mathrm{Re}_{ff} \geq \mathrm{Re}_{ff\infty})$

$$\frac{\dot{\varepsilon} D_h}{\mu_f} = 1.2\times10^3\,\mathrm{Re}_f^{-0.5}\,\mathrm{Re}_{ff\infty}^{-0.25}\,\mathrm{We}_g^{-1.5}\left(\mathrm{Re}_{ff} - \mathrm{Re}_{ff\infty}\right)^2 + 6.6\times10^{-7}\,\mathrm{Re}_f^{0.74}\,\mathrm{Re}_{ff}^{0.185}\,\mathrm{We}_g^{0.925}\left(\frac{\mu_g}{\mu_f}\right)^{0.26} \tag{19}$$

For the equilibrium region $(\mathrm{Re}_{ff} < \mathrm{Re}_{ff\infty})$

$$\frac{\dot{\varepsilon}_e D_h}{\mu_f} = 6.6\times10^{-7}\,\mathrm{Re}_f^{0.74}\,\mathrm{Re}_{ff}^{0.185}\,\mathrm{We}_g^{0.925}\left(\frac{\mu_g}{\mu_f}\right)^{0.26} \tag{20}$$

where, the gas phase Weber number (We_g) and liquid phase Reynolds numbers are defined as follows

$$\mathrm{We}_g = \frac{\rho_g j_g^{\,2} D_h}{\sigma}\left(\frac{\Delta\rho}{\rho_g}\right)^{1/3} \tag{21}$$

$$\mathrm{Re}_{ff} = \frac{\rho_f j_{ff} D_h}{\mu_f} = \frac{\rho_f j_f (1-E) D_h}{\mu_f} \tag{22}$$

$$\mathrm{Re}_{ff\infty} = \frac{\rho_f j_{ff_\infty} D_h}{\mu_f} = \mathrm{Re}_f\left(1 - E_\infty\right) \tag{23}$$

Here, j_{ff} is the superficial film velocity, j_{ff_∞} is the equilibrium superficial film velocity. E and E_∞ are the entrainment fraction and equilibrium entrainment fraction, respectively.

2.2.2. Droplet deposition rate

The amount of entrained droplets represents the integral effects of entrainment to the gas core as well as deposition to the liquid film. The deposition rate $\dot{d}$ can be linearly related to the droplet concentration in the gas core by [45-48]

$$\dot{d} = k_d C \tag{24}$$

where, $\dot{d}$, k_d and C are the droplet deposition rate, mass transfer coefficient, and mass concentration in the gas core, respectively. Okawa and Kataoka [49] compared many existing correlations with available experimental databases. The authors found that the deposition rate increases with the superficial gas velocity under the condition of low droplet concentration, while the influence of j_g on the deposition rate is not significant for high droplet concentration. The droplet deposition rate for both low and high droplet mass concentrations in gas core can be expressed by

For $C^* < 0.15$ (Low concentration)

$$k_d = 0.17 u_f \tag{25}$$

where, u_f is the friction velocity calculated using Fanning friction factor.

For $C^* \geq 0.15$ (High concentration)

$$k_d \sqrt{\frac{\rho_g D_h}{\sigma}} = \min\left[0.19\left(C^*\right)^{-0.2}, 0.105\left(C^*\right)^{-0.8}\right] \tag{26}$$

where $C^* = C/\rho_g$.

2.2.3. Film and droplet evaporation rate

The evaluation of the evaporation and condensation rates is critical to the mass transport and heat transfer in transients of two-phase thermosyphons and heat pipes. The liquid film evaporation rate based on the free molecular flow mass flux model presented by Collier [15] can be expressed by

$$\dot{\gamma}_f = \left(\frac{M}{2\pi RT}\right)^{0.5} (p_l - p_v) \tag{27}$$

where, *M* is the molecular weight, *R* is the universal gas constant. $\dot{\gamma}_f$ is positive when liquid pressure is greater than vapor pressure, and vice versa. This model has been widely applied for analyzing the transient characteristics of a micro heat pipe [50,51]. A similar model based on classical kinetic theory for evaluating the net evaporative mass flux can be given by [52]

$$\dot{\gamma}_f = \left(\frac{2\zeta}{2-\zeta}\right)\left(\frac{M}{2\pi RT}\right)^{0.5}\left(\frac{p_l}{\sqrt{T_l}} - \frac{p_v}{\sqrt{T_v}}\right) \tag{28}$$

where ζ is the accommodation coefficient and changes regarding working fluid and temperature ranges. It should be noted that the evaporation rates from Eqs. (27) and (28) are zero under the assumption of the mechanical equilibrium and thermal equilibrium conditions using saturated pressures and temperatures.

2.2.4. Liquid film thickness

In the case of modeling the two-phase thermosyphon without a wick, the determination of the film thickness δ is the key to determining the gas core flow area, which requires another constitutive equation. Several film thickess correlations have been proposed in the literature [33,53,54]. Wallis [29] gave a simple film thickness correlation based on the dimensionless falling film thickness defined by

$$\delta^* = \frac{\delta g^{1/3}\left(\rho_f - \rho_g\right)^{1/3}\rho_f{}^{1/3}}{\mu_f{}^{2/3}} \tag{29}$$

And δ^* can be evaluated by

$$\delta^* = \begin{cases} 0.909\,\mathrm{Re}_f{}^{1/3}, \mathrm{Re}_f \le 1000 \\ 0.063\,\mathrm{Re}_f{}^{2/3}, \mathrm{Re}_f > 1000 \end{cases} \tag{30}$$

To better account for the entrainment limit, Ju et al. recently proposed a functional form for average film thickness as [55,56]

$$\delta = \delta_{\max}\tanh\left(C\mathrm{We}_f{}^{a}\mathrm{We}_g{}^{b}\mathrm{N}_{\mu_f}{}^{c}\right) \tag{31}$$

For air-water two-phase flows, Eq. (31) can be determined based on many experimental datasets. The final form can be given by

$$\delta = 0.071D\tanh\left(14.22\mathrm{We}_f{}^{0.24}\mathrm{We}_g{}^{-0.47}\mathrm{N}_{\mu_f}{}^{0.21}\right) \tag{32}$$

where, the maximum film thickness $\delta_{\max}$ is $0.071D$ derived from analyzing experimental data. It should be noted that the above-mentioned constitutive equations were developed and validated based on air-water or

steam-water experiments. Large uncertainties could be introduced if these correlations are directly applied to other working fluids such as liquid metals in the thermosyphons or heat pipes in the microreactors. Thus, more experimental databases will be needed from newly designed test facilities simulating high-temperature operating conditions in the microreactors.

2.2.5. Capillary pressure

Wicks can be used to improve boiling and evaporation heat transfer in the evaporator section and therefore to increase heat flux. Considering the operation of a heat pipe, evaporation of the liquid wetting the wick surface will create a concave meniscus in wick pores in the evaporator. The capillary pressure is defined as the pressure difference between the vapor and liquid due to the action of surface tension acting on the liquid. The capillary pressure can be calculated by the Laplace and Young equation as [1]

$$p_{cap} = \sigma\left(\frac{1}{R_1} + \frac{1}{R_2}\right) \tag{33}$$

where, R_1 and R_2 are the principal radii of the meniscus. For a cylindrical porous wick, R_1 and R_2 can be equal. Thus, Eq. (33) can be given by

$$p_{cap} = \frac{2\sigma\cos\theta}{r} \tag{34}$$

where, r and θ are the radius of the cylindrical pore and the wetting angle, respectively [1]. For the wicks of cylindrical pores, the capillary pressure will reach the maximum values when the wetting angle is zero. The maximum capillary pressure can be expressed by [1]

$$p_{cm} = \frac{2\sigma}{r} = \frac{2\sigma}{r_c} \tag{35}$$

here, r_c is the effective capillary radius. In the condenser, condensation of liquid causes flooding in the wick pores and negligible menisci curvature. Normally, the capillary pressure in the condenser will be smaller than that in the evaporator.

Heat pipe design requires optimizing the competing effects of effective capillary radius and permeability regarding wick structures. A small effective capillary radius is desired for increased capillary pumping, yet this also restricts liquid flow, thereby increasing the viscous pressure drop. The type of wick structure used and its properties, are crucial in the successful design of heat pipes. Heat pipes in microreactors usually have a high aspect ratio that their lengths are around two orders of magnitude greater than their outer pipe diameters. Since the liquid flow path is very long, it is desirable to have a capillary structure with high permeability with the heat pipe oriented vertically to utilize gravity and minimize viscous losses [7]. Therefore, wick structures such as annulus-screen, artery, or composite structures such as screen-covered axial grooves are more appropriate for heat pipe cooled microreactor applications, as they offer high permeability while limiting entrainment from the liquid [57]. Some literature reported the annulus-screen wicks designed for heat pipes in microreactors [7,58]. On the other hand, the wick structures with low effective capillary radii and permeabilities, such as sintered metal powder and wrapped screen wicks, characterize high capillary pumping capabilities. These wick structures are more suitable for use in shorter heat pipes or with horizontal, non-gravity aiding orientations or microgravity conditions.

2.3. High-temperature Working Fluids

High temperature working fluids such as alkali metals are used in heat pipes in microreactors, which are designed to produce thermal power of less than 20 MWt for remote installations [7]. Liquid metals show different boiling characteristics than other fluids such as water due to the differences in physical properties [58]. Table 1 compares characteristic material properties determining boiling behavior for three liquids: water (H_2O), sodium (Na), and potassium (K). Surface tension and latent heat determine the nucleation process and superheat, along with the heating surface characteristics. The nucleation superheats for liquid metals tend to be higher than those for ordinary fluids, which delay the boiling of liquid metals. Heat transfer and pressure drops are closely related to two-phase flow patterns. Due to the great difficulties of performing experiments using liquid metals, there exist very few flow visualization data on flow patterns for liquid metals. Generally, the flow patterns are similar to the case of water consisting of bubbly flow, slug flow, annular flow, and mist flow in a uniformly heated vertical channel [59]. In addition, the liquid droplets were observed to deposit to the wall from a series of snapshots of X ray images [60]. Another experimental study on sodium boiling in a single-pin annular channel showed a similar flow pattern transitions from bubbly flow to slug flow and then to annular flow [61]. Therefore, it can be expected that the flow patterns inside a heat pipe for liquid metals and for low-temperature fluids will also be similar. It should be noted that heat transfer correlations developed based on ordinary fluids could result in relatively

large uncertainties for predicting liquid-metal boiling. A detailed description of various boiling mechanisms can be found in Refs [59,62,63].

Table 1. Comparison of characteristic physical properties determining boiling behavior [64]

	H_2O	**Na**	**K**
Pressure (kPa)	100	100	100
Boiling point (°C)	99.6	877.8	760.7
Surface tension (N/m)	0.059	0.115	0.063
Latent heat (kJ/kg)	2257.4	3893.2	1925.0
Liquid specific heat (kJ/kg-K)[1]	4.22	1.28	0.85
Liquid thermal conductivity (W/m-K)	0.679	52.3	30.4
Liquid density (kg/m^3)	958.6	742.8	663.8
Liquid to vapor density ratio (-)	1624.8	2776.3	1349.9
Liquid Prandtl number (-)	1.76	0.0038	0.0037

2.4. Dimensionless Parameters

Scaling analysis for passive systems such as natural circulation thermal-hydraulics and heat pipes are challenging due to the coupling of the heat transfer and flow properties [66]. Dimensionless parameters are used for analyzing physics such as fluid properties, flow regimes, heat transfer mechanisms, and dynamics in a system during the scaling analysis. These numbers are important for the development of scalable modeling techniques as well as designing experimental test facilities. Heat pipe operation involves many physical phenomena such as phase-change heat transfer, two-phase flows, compressibility, entrainment, and capillary effects. A variety of dimensionless numbers can be obtained by non-dimensionalizing the governing equations describing two-phase flows in heat pipes. Table 2 summarizes the dimensionless parameters that can be used for heat pipe analysis.

[1] Liquid specific heat data from reference [65] at 1 atm.

Table 2: Summary of dimensionless parameters.

Dimensionless Parameter	Expression	Interpretation
Aspect ratio	$a = L / D$	Ratio of axial length to inner pipe diameter
Reynolds number	$\mathrm{Re}_k = \rho_k v_k D_{h,k} \big/ \mu_k$	Ratio of inertial forces to viscous forces
Euler number	$\mathrm{Eu}_k = \dfrac{\Delta p_k}{\rho_k v_k}$	Ratio of pressure forces to inertial force
Mach number	$\mathrm{Ma} = \dfrac{v_g}{v_s}$	Ratio of gas velocity to sonic velocity
Weber number	$\mathrm{We}_k = \dfrac{\rho_k v_k^2 D_{h,k}}{\sigma}$	Ratio of inertial forces to surface tension forces
Modified gas Weber number [39]	$\mathrm{We}_g^{'} = \dfrac{\rho_g v_g^2 D_{h,g}}{\sigma}\left(\dfrac{\Delta\rho}{\rho_g}\right)^{1/3}$	Ratio of inertial to surface tension forces
Froude number	$\mathrm{Fr}_k = \dfrac{v_k^2}{gL}$	Ratio of inertial forces to gravitational forces
Prandtl number	$\mathrm{Pr}_k = \mu_k c_{p,k} \big/ k_k$	Ratio of momentum diffusivity to thermal diffusivity
Péclet number	$\mathrm{Pe}_k = \dfrac{\rho_k v_k \Delta h_k D_{h,k}}{k_k \Delta T_k}$	Ratio of heat convection to heat conduction
Density ratio	ρ_f / ρ_g	Density ratio of liquid to gas
Viscosity ratio	μ_f / μ_g	Viscosity ratio of liquid to gas
Dimensionless time	$t v_f / L$	Scaling transient phenomena

Many dimensionless parameters described in Table 2 are widely used by researchers in mechanical and nuclear engineering. The uncommon ones deserve some elaboration as follows. The modified gas Weber number is based on the onset of entrainment criteria developed by Ishii and Grolmes [39]. In addition, the Laplace length $\sqrt{\sigma \big/ \left(g\Delta\rho\right)}$, a parameter independent of pipe geometry, is proposed as a more suitable length scale for analyzing entrainment phenomena compared to the pipe diameter according to Wang et al., since entrainment is a local phenomenon [67].

An example to choosing dimensionless parameters for scaling analysis can be given when studying entrainment phenomenon in a heat pipe. Section 2.2.1 shows the dependence of the entrainment rate on the liquid viscosity number, film Reynolds number and the modified gas Weber number. Additionally, Ju et al. have shown the importance of the liquid Weber number on the film thickness as described in Section 2.2.4 [55]. This suggests the parameter's importance on the liquid film properties. It is also clear based on Eqs. (20) and (32) that the importance of the gas Weber number is the greatest on the entrainment rate and the film thickness. These parameters can thus be used to scale a prototype for the study of entrainment phenomena.

3. CONCLUSIONS

The modeling of countercurrent annular two-phase flow is essential to predicting the normal operation and transients in the two-phase heat pipes and thermosyphons for fission heat removal in nuclear microreactors. However, there exists no agreement on two-phase flow modeling approaches to be implemented for heat pipe applications in nuclear reactors. This paper presents the most comprehensive one-dimensional two-phase three-field modeling framework including conservation equations and constitutive models for the liquid film, vapor, and droplets. Specifically, required constitutive equations due to the introduction of the droplet field are thoroughly discussed. The developed modeling framework and constitutive models and correlations will provide a modeling basis for ongoing research activities and future licensing of heat pipe-cooled microreactors. It should be noted that most of the existing correlations developed have been verified and validated based on air-water or steam-water two-phase flow experiments. For the applications in the microreactors, high temperature working fluids such as sodium or potassium will be used in the heat pipes. It is critical to design new heat pipe test facilities including advanced wick designs for experiments using prototype fluids under high-temperature conditions or other surrogate fluids based on a comprehensive scaling analysis. A discussion on liquid metal working fluids and dimensionless parameters for heat pipe scaling analysis and model development were given to provide instructions on designing new test facilities. More experimental data will be needed to validate and improve various constitutive models and correlations on material properties, heat transfer coefficients, and flow dynamics for the two-phase heat pipes in the future. The validated heat pipe constitutive models can also be implemented by modern computational tools currently being developed in national laboratories for microreactors.

NOMENCLATURE

Latin

a	aspect ratio [-]
C	droplet concentration in the gas core [kg/ m^3]
$\dot{d}$	droplet deposition rate per unit film surface area [kg/m^2-s]
D	pipe diameter [m]
D_h	hydraulic diameter [m]
E	entrainment fraction [-]
f	friction factor [-]
g	gravitational acceleration [m/s^2]
h	enthalpy [J/kg]
c_p	specific heat at constant pressure [J/kg-K]
j	volumetric velocity [m/s]
k	thermal conductivity [W/m-K]
k_{eff}	effective thermal conductivity [W/m-K]
k_d	mass transfer coefficient [m/s]
K	wick permeability [m^2]
M	molecular weight [g/mol]
M_{iD}	drag force term between droplet and gas [Pa/m]
M_{wick}	drag force term between the liquid and wick [Pa/m]
p	pressure [Pa]
p_{cap}	capillary pressure [Pa]
p_{cm}	maximum capillary pressure [Pa]
q''	heat flux [W/m^2]
r	radius [m]
L	length [m]
R	universal gas constant [-]
t	time variable [s]
T	temperature [K]
v	velocity [m/s]
v_s	sonic velocity [m/s]
z	axial displacement variable [m]
Eu	Euler number [-]

Fr Froude number [-]

Ma Mach number [-]

$N_{\mu f}$ viscosity number [-]

Pe Péclet number [-]

Pr Prandtl number [-]

Re Reynolds number [-]

We Weber number [-]

Greek symbol

α void fraction [-]

α_d droplet fraction in the gas core region [-]

$\dot{\gamma}_f$ film evaporation rate per unit film surface area [kg/m^2-s]

$\dot{\Gamma}_d$ droplet evaporation rate per unit vapor-droplet mixture volume [kg/m^3-s]

Δh enthalpy drop [J/kg]

Δp pressure drop [Pa]

ΔT temperature drop [K]

$\Delta \rho$ density difference [kg/m^3]

δ wick thickness or film thickness [m]

ε wick porosity [-]

ε_i liquid area fraction at the wick-gas interface [-]

ε_w liquid area fraction at the wall [-]

$\dot{\varepsilon}$ droplet entrainment rate per unit film surface area [kg/m^2-s]

ζ accommodation coefficient [-]

μ liquid viscosity [Pa-s]

ρ density [kg/m^3]

σ surface tension [N/m]

τ_i interfacial shear stress between liquid and gas [Pa]

$\tau_{i,wick}$ shear stress between gas and wick at the interface [Pa]

τ_w wall shear stress [Pa]

Subscript

d droplet

di droplet interface

f liquid film or liquid

fi liquid film interface

g gas phase

i interface

k liquid or gas phase

l liquid

v vapor

w wall

REFERENCES

1. S. W. Chi, *Heat Pipe Theory and Practice: A Sourcebook*, Hemisphere Publishing Corporation, Washington (1976).
2. G. P. Peterson, *An Introduction to Heat Pipes: Modeling, Testing, and Applications*, John Wiley & Sons, New York (1994).
3. A. Faghri, *Heat Pipe Science and Technology*, Taylor & Francis, Washington, DC (1995).
4. B. Zohuri, *Heat Pipe Design and Technology - Modern Applications for Practical Thermal Management (Second Edition)*, Springer, Switzerland (2016).
5. P. Sabharwall, "Engineering Design Elements of a Two-Phase Thermosyphon to Transfer NGNP Thermal Energy to a Hydrogen Plant," Idaho National Laboratory, INL/EXT-09-15383 (2009).
6. P. R. Mcclure, D. I. Poston, V. R. Dasari, and R. S. Reid, "Design of Megawatt Power Level Heat Pipe Reactors," Los Alamos National Laboratory, LA-UR-15-28840 (2015).
7. J. W. Sterbentz, J. E. Werner, A. J. Hummel, J. C. Kennedy, R. C. O'Brien, A. M. Dion, R. N. Wright, and K.P. Ananth, "Preliminary Assessment of Two Alternative Core Design Concepts for the Special Purpose Reactor," Idaho National Laboratory, INL/EXT-17-43212 (2018).
8. S.M. Bragg-Sitton, "Heat Pipe Reactor Dynamic Response Tests: SAFE-100a Reactor Core Prototype," Proc. of the Space Nuclear Conference, San Diego, California, June 5-9 (2005).
9. S. M. Bragg-Sitton, "Analysis of Space Reactor System Components: Investigation through Simulation and Non-nuclear Testing," Dissertation, University of Michigan, United States (2004).
10. C. Muller and P. Tsvetkov, "A Review of Heat-pipe Modeling and Simulation Approaches in Nuclear Systems Design and Analysis," *Ann. Nucl. Energy*, **160**, 108393 (2021).
11. P. Sabharwall, V. Utgikar, and F. Gunnerson, "Dimensionless Numbers in Phase-Change Thermosyphon and Heat-Pipe Heat Exchangers," *Nucl. Technol.* **167** (2), pp. 325-332 (2009).

12. S.-W. Chen et al., "Modeling and Analyses of Boiling and Capillary Limitations for Micro Channel Wick Structures," *J. Mechanics*, **32** (3), pp. 357-368 (2016).
13. C. Muller and P. Tsvetkov, "Novel Design Integration for Advanced Nuclear Heat-pipe Systems," *Ann. Nucl. Energy*, **141**, 107324 (2020).
14. J. G. Reed and C. L. Tien, "Modeling of the Two-Phase Closed Thermosyphon," *J. Heat Transfer,* **109** (3), pp. 722-730 (1987).
15. J. C. Collier, *Convective Boiling and Condensation*, McGraw-Hill, New York (1982).
16. C. Harley and A. Faghri, "Complete Transient Two-Dimensional Analysis of Two-Phase Closed Thermosyphons Including the Falling Condensate Film," *J. Heat Transfer,* **116** (2), pp. 418-426 (1994).
17. J-M. Tournier, and M. S. El-Genk, "A Heat Pipe Transient Analysis Model," *Int. J. of Heat and Mass Transfer*, **37**(5), pp. 753-762 (1994).
18. J-M. Tournier, and M. S. El-Genk, "A Vapor Flow Model for Analysis of Liquid-Metal Heat Pipe Startup from a Frozen State," *Int. J. of Heat and Mass Transfer,* **39**(18), pp 3767-3780 (1996).
19. Z.J. Zuo and A. Faghri, "A Network Thermodynamic Analysis of the Heat Pipe," *Int. J. Heat Mass Transfer*, **41**(11), pp. 1473-1484 (1998).
20. G. Hu, R. Hu, and L. Zou, "Development of Heat Pipe Reactor Modeling in SAM," Argonne National Laboratory, ANL/NSE-19/9 (2019).
21. C. Zhang, S. Wu, and F. Yao, "Evaporation Regimes in an Enclosed Narrow Space," *Int. J. of Heat and Mass Transfer*, **138**, pp. 1042-1053 (2019).
22. C. Zhang, F. Yu, X. Li, and Y. Chen, "Gravity-capillary Evaporation Regimes in Microgrooves," *AIChE J.*, **65**(3), pp. 1119-1125 (2019).
23. X. Liu, Y. Chen, and M. Shi, "Dynamic Performance Analysis on Start-up of Closed-loop Pulsating Heat Pipes (CLPHPs)," *Int. J. of Therm. Sci.*, **65**, pp. 224-233 (2013).
24. M. Ishii, *Thermo-Fluid Dynamic Theory of Two-Phase Flow*, Eyrolles, Paris (1975).
25. M. Ishii and K. Mishima, "Two-fluid Model and Hydrodynamic Constitutive Relations," *Nucl. Eng. Des.*, **82**(2-3), pp. 107-126 (1984).
26. C. Morel, "Modeling Approaches for Strongly Non-homogeneous Two-phase Flows," *Nucl. Eng. Des.*, **237** (11), pp. 1107-1127 (2007).
27. R. T. Lahey Jr and D. A. Drew, "The Analysis of Two-phase Flow and Heat Transfer using a Multidimensional, Four field, Two-fluid Model," *Nucl. Eng. Des.*, **204** (1-3), pp. 29-44 (2001).
28. Y. Liu, J. D. Talley, K. J. Hogan, and J. R. Buchanan, "A Generic Framework for Multi-Field Two-Phase Flow based on the Two-Fluid Model," *Prog. Nucl. Energ.*, **94**, pp. 80-92, Jan. 2017.
29. G. B. Wallis, *One-dimensional Two-phase Flow*, McGraw-Hill, New York (1969).
30. G. F. Hewitt, and N. S. Hall-Taylor, *Annular Two-phase Flow*, Pergamon Press, New York (1970).

31. M. Ishii and T. Hibiki, *Thermo-Fluid Dynamics of Two-Phase Flow, Second edition*, Springer, New York (2011).
32. E. O. Moeck and J. W. Stachiewicz, “A Droplet Interchange Model for Annular-dispersed, Two-phase Flow,” *Int. J. Heat and Mass Transfer*, **15**(4), pp. 637-653 (1972).
33. W. H. Henstock and T. J. Hanratty, “The Interfacial Drag and the Height of the Wall Layer in Annular Flows,” *AIChE J.*, **22**(6), pp. 990-1000 (1976).
34. J. Asali, T. t. Hanratty, and P. Andreussi, “Interfacial Drag and Film Height for Vertical Annular Flow,” *AIChE J.*, **31**(6), pp. 895-902 (1985).
35. T. Fukano and T. Furukawa, “Prediction of the Effects of Liquid Viscosity on Interfacial Shear Stress and Frictional Pressure Drop in Vertical Upward Gas–liquid Annular Flow,” *Int. J. of Multiphase Flow*, **24**(4), pp. 587-603 (1998).
36. L. B. Fore, S. G. Beus, and R. C. Bauer, “Interfacial Friction in Gas-liquid Annular Flow: Analogies to Full and Transition Roughness,” *Int. J. of Multiphase Flow*, **26**(11), pp. 1755-1769 (2000).
37. R. J. Belt, J. M. C. Van't Westende, and L. M. Portela, “Prediction of the Interfacial Shear-stress in Vertical Annular Flow,” *Int. J. of Multiphase Flow*, **35**(7), pp. 689-697 (2009).
38. K. M. Kim and I. C. Bang, “Thermal-hydraulic Phenomena inside Hybrid Heat Pipe-control Rod for Passive Heat Removal,” *Int. J. Heat and Mass Transfer*, **119**, pp. 472-483 (2018).
39. M. Ishii and M. A. Grolmes, “Inception Criteria for Droplet Entrainment in Two-phase Concurrent Film Flow,” *AIChE J.*, **21**(2), pp. 308-318 (1975).
40. M. A. Lopez de Bertodano, A. Assad, and S. G. Beus, “Experiments for Entrainment Rate of Droplets in the Annular Regime,” *Int. J. of Multiphase Flow*, **27**(4), pp. 685-699 (2001).
41. M. A. Lopez de Bertodano, C. S. Jan, and S. G. Beus, “Annular Flow Entrainment Rate Experiment in a Small Vertical Pipe,” *Nucl. Eng. Des.*, **178**(1), pp. 61-70 (1997).
42. T. Okawa and I. Kataoka, “Correlations for the Mass Transfer Rate of Droplets in Vertical Upward Annular Flow," *Int. J. Heat and Mass Transfer*, **48**(23-24), pp. 4766-4778 (2005).
43. L. Pan and T. J. Hanratty, “Correlation of Entrainment for Annular Flow in Vertical Pipes,” *Int. J. of Multiphase Flow*, 28(3), pp. 363-384 (2002).
44. I. Kataoka and M. Ishii, “Entrainment Rate in Annular Two-Phase Flow” Argonne National Laboratory, ANL/RAS/LWR 82-1, USA (1982).
45. T. Okawa, T. Kitahara, K. Yoshida, T. Matsumoto, and I. Kataoka, “New Entrainment Rate Correlation in Annular Two-phase Flow Applicable to Wide Range of Flow Condition,” *Int. J. Heat and Mass Transfer*, **45**(1), pp. 87-98 (2002).
46. I. I. Paleev and B. S. Filippovich, "Phenomena of Liquid Transfer in Two-phase Dispersed Annular Flow," *Int. J. Heat and Mass Transfer*, **9**(10), pp. 1089-1093 (1966).

47. S. Schadel, G. Leman, J. Binder, and T. Hanratty, “Rates of Atomization and Deposition in Vertical Annular Flow," *Int. J. of Multiphase Flow*, **16**(3), pp. 363-374 (1990).
48. S. Sugawara, “Analytical Prediction of CHF by FIDAS Code Based on Three-fluid and Film-dryout Model,” *J. Nucl. Sci. Technol.*, **27**(1), pp. 12-29 (1990).
49. T. Okawa and I. Kataoka, “Correlations for the Mass Transfer Rate of Droplets in Vertical Upward Annular Flow,” *Int. J. Heat and Mass Transfer,* **48**, pp. 4766-4778 (2005).
50. D. Wu and G. P. Peterson, “Investigation of the Transient Characteristics of a Micro Heat Pipe,” *J. Thermophysics*, **5**(2), pp. 129-134 (1991).
51. Z. Xu, Y. Zhang, B. Li, and J. Huang, “Modeling the Phase Change Process for a Two-phase Closed Thermosyphon by Considering Transient Mass Transfer Time Relaxation Parameter,” *Int. J. Heat and Mass Transfer*, **101**, pp. 614-619 (2016).
52. M. L. Hall and J. M. Doster, “A Sensitivity Study of the Effects of Evaporation/Condensation Accommodation Coefficients on Transient Heat Pipe Modeling,” *Int. J. Heat and Mass Transfer,* **33** (3), pp. 465-481 (1990).
53. D. F. Tatterson, J. C. Dallman, and T. J. Hanratty, “Drop Sizes in Annular Gas-liquid Flows,” *AIChE Journal*, **23**(1), pp. 68-76 (1977).
54. T. Fukano and T. Furukawa, “Prediction of the Effects of Liquid Viscosity on Interfacial Shear Stress and Frictional Pressure Drop in Vertical Upward Gas–liquid Annular Flow,” *Int. J. of Multiphase Flow*, **24**(4), pp. 587-603, 1998.
55. P. Ju, C. S. Brooks, M. Ishii, Y. Liu, T. Hibiki, “Film Thickness of Vertical Upward Co-current Adiabatic Flow in Pipes,” *Int. J. Heat and Mass Transfer,* **89**, pp. 985-995 (2015).
56. P. Ju, Y. Liu, C. S. Brooks, and M. Ishii, “Prediction of Interfacial Shear Stress of Vertical Upward Adiabatic Annular Flow in Pipes,” *Int. J. Heat and Mass Transfer*, **133**, pp. 500-509 (2019).
57. I. Yilgor and S. Shi, “Modeling and Investigation of Various Types of Wick Structures in Heat Pipe Micro Reactor Applications,” *Trans. Am. Nucl. Soc.*, **124**(1), pp. 710-713 (2021).
58. J-M. Tournier, and M. S. El-Genk. “A Vapor Flow Model for Analysis of Liquid-Metal Heat Pipe Startup from a Frozen State,” *Inter. J. of Heat and Mass Transfer*, **39**(18), pp. 3767-3780 (1996).
59. H.M. Kottowski and C. Savatteri, “Fundamentals of Liquid Metal Boiling Thermohydraulics,” *Nucl. Eng. Des.*, **82**, pp. 281-304 (1984).
60. H. Schmucker and U. Grigull, “Boiling of Mercury in a Vertical Tube Under Forced-Flow Conditions,” *Prog. in Heat and Mass Transfer*, **7**, pp. 363-376 (1973).
61. Y. Kikuchi, K. Haga, and T. Takahashi, “Experimental Study of Steady-State Boiling of Sodium Flowing in a Single-Pin Annular Channel,” *J. Nucl. Sci. Technol.*, **12**(2), pp. 83-91 (1975)
62. L.S. Tong and Y.S. Tang, *Boiling Heat Transfer and Two-phase Flow (2nd Edition)*, CRC Press, (1997).

63. P. Sabharwall, V. Utgikar, A. Tokuhiro, and F. Gunnerson, “Design of Liquid Metal Phase Change Heat Exchanger for Next-Generation Nuclear Plant Process Heat Application,” *J. Nucl. Sci. Technol.*, **46**(6), pp. 534-544 (2009).
64. P. J. Brennan, and E. J. Kroliczek, *Heat Pipe Design Handbook: Volume II*, B and K Engineering, Inc., Towson, MD (1979).
65. O. E. Dwyer, *Boiling Liquid-Metal Heat Transfer*, American Nuclear Society, Hinsdale, IL (1976)
66. M. Ishii, and I. Kataoka, “Scaling Laws for Thermal-Hydraulic System Under Single Phase and Two-Phase Natural Circulation,” *Nucl. Eng. Des.* **81**(3), pp. 411-425 (1984).
67. G. Wang, P. Sawant, and M. Ishii, “A New Entrainment Rate Model for Annular Two-Phase Flow,” *Int. J. of Multiphase Flow*, **124**,103185 (2020).